HHS Public Access

Author manuscript

Mater Today Chem. Author manuscript; available in PMC 2020 December 01.

Published in final edited form as:

Mater Today Chem. 2019 December ; 14: . doi:10.1016/j.mtchem.2019.08.004.

POLYBENZIMIDAZOLE NANOFIBERS FOR NEURAL STEM CELL CULTURE

Fábio F. F. Garrudo[a,b,c], **Ranodhi N. Udangawa**[a], **Pauline R. Hoffman**[a], **Laura Sordini**[b,c,d], **Caitlyn A. Chapman**[a], **Paiyz E. Mikael**[a], **Flávio A. Ferreira**[b,c], **João C. Silva**[a,b,c], **Carlos A. V. Rodrigues**[b,c], **Joaquim M. S. Cabral**[b,c], **Jorge M. F. Morgado**[d], **Frederico C. Ferreira**[b,c], **Robert J. Linhardt**[a,*]

[a]Center for Biotechnology and Interdisciplinary Studies, Department of Chemistry and Chemical Biology, Rensselaer Polytechnic Institute, Troy, New York, 12180-3590, United States.

[b]Department of Bioengineering and iBB – Institute for Bioengineering and Biosciences, Instituto Superior Técnico, Universidade de Lisboa, Av. Rovisco Pais, P-1049-001 Lisboa , Portugal.

[c]The Discoveries Centre for Regenerative and Precision Medicine, Lisbon Campus, Instituto Superior Técnico, Universidade de Lisboa, Av. Rovisco Pais, P-1049-001 Lisboa, Portugal.

[d]Department of Bioengineering and Instituto de Telecomunicações, Instituto Superior Técnico, Universidade de Lisboa, P-1049-001 Lisboa, Portugal.

Abstract

Neurodegenerative diseases compromise the quality of life of increasing numbers of the world's aging population. While diagnosis is possible no effective treatments are available. Strong efforts are needed to develop new therapeutic approaches, namely in the areas of tissue engineering and *deep brain stimulation* (DBS). Conductive polymers are the ideal material for these applications due to the positive effect of conducting electricity on neural cell's differentiation profile. This novel study assessed the biocompatibility of polybenzimidazole (PBI), as electrospun fibers and after being doped with different acids. Firstly, doped films of PBI were used to characterize the materials' contact angle and electroconductivity. After this, fibers were electrospun and characterized by SEM, FTIR and TGA. Neural Stem Cell's (NSC) proliferation was assessed and their growth rate and morphology on different samples was determined. Differentiation of NSCs on PBI - CSA fibers was also investigated and gene expression (SOX2, NES, GFAP, Tuj1) was assessed through Immunochemistry and qPCR. All the samples tested were able to support neural stem cell (NSC) proliferation without significant changes on the cell's typical morphology.

*Corresponding Author: linhar@rpi.edu.

AUTHORS CONTRIBUTIONS

The study was performed by FFFG, RNU, PH, LS, CAC and FAF. The original idea was proposed by FCF. Experimental plan was designed by FFFG, PEM, JMFM, FCF and RJL. Preliminary data experiments were performed by FFFG, JCS and CAVR. JMSC, JMFM, FCF and RJL provided lab space. The manuscript was written by FFFG, RNU, LS, PEM, FAF, JCS, CAVR, JMFM, FCF and RJL.

CONFLITS OF INTEREST

No conflicts of interest to declare.

Successfully differentiation of NSCs towards neural cells on PBI – CSA fibers was also achieved. This promising PBI fibrous scaffold material is envisioned to be used in neural cell engineering applications, including scaffolds, *in vitro* models for drug screening and electrodes.

Keywords

Scaffolds; Electrospinning; Conductive polymers; Biocompatibility; Neural engineering; Regenerative medicine

1. INTRODUCTION

Neurological disorders affect the quality of life and autonomy of patients, their families and society in general. They involve the irreversible loss of neural tissue, which in turn causes cognitive loss, movement impairment and dementia. With the increase of aging population, the social and economic burden of these diseases will rise. Current available therapies can only alleviate the symptoms, they cannot rescue or regenerate neural cells or cellular function [1].

The central nervous system has a high electrical activity. The use of electricity to direct the development *in vitro* of axons and neurites of neural cells has been widely studied [2,3]. *In vivo,* this can be achieved through Deep Brain Stimulation (DBS), in which the brain tissue is electrically stimulated using temporary and directly implanted probes [4]. This technique allows not only the recording of brain activity but also the direct application of electricity to the brain tissue. The effects of DBS on neurological diseases, especially neurogenerative ones such as Alzheimer and Parkinson's disease, are promising and require complete clinical studies to assess their full clinical value [4-7]. Some challenges persist, including the fact that clinical assay must be done directly in humans [5]. These means that the materials used for these probes must be biocompatible, allowing total integration of it in the brain tissue without damaging it, and be electroconductive.

The combination of electrical stimulation and cell supportive biomaterials is useful in enhancing the phenotype and functionality of *in vitro* cultured cells[3,8- 10]. This strategy is largely used in tissue engineering, which can also be applied to the development of disease model platforms or transplants for direct integration in brain tissue [11]. The physico-chemical and mechanical properties of these biomaterials have to be similar to the native tissue, boosting biocompatibility through successful tissue integration, for these biomaterials to be used in neural tissue therapies [12,13]. In fact, studies report that transplanted stiffer materials (e.g., metals) cause more tissue damage than softer materials such as polymers, hindering their performance in the long run [12,14,15].

Polymers can be shaped to better mimic the natural Extra-Cellular Matrix (ECM) environment of the target tissue [3,13]. This includes diverse forms such as films[2], hydrogels [16,17] and fibers [18,19]. In particular, electroconductive polymers are a very interesting option since they are available to conduct electricity directly to adhered cells, benefiting their growth and differentiation [3,20,21]. However, conductive polymers are more versatile, have a lower cost, and can be easily tailored/functionalized [22-24]. Some

examples of conductive polymers include polypyrrole (PPy) [25], polyaniline (PANI) [26], and polyethylenedioxythiophene (PEDOT) [2].

In the last years electrospun fibers gained a lot of attention mainly due to nanofibers being able to structurally mimic the fibrillar structures present in natural ECM [27,28]. Fibers made of conductive polymers, such as PPy and PANI, have been produced and were successfully demonstrated not only to be biocompatible but also increased the differentiation of Neural Stem Cells (NSC) when electricity was applied [29-31]. However, these polymers can only be electrospun using non- conductive carrier polymers (e.g., PCL). This decreases the electroconductivity of the resulting fibers when compared with cast films of the neat materials. Furthermore, the process compromises the direct injection of electrical current and minimizes the positive effects of electrical stimulation of the cells [32,33].

Poly-benzimidazole (PBI) is a fully aromatic heterocyclic conductive polymer. Many authors have described PBI as a chemically stable polymer and have shown that these imidazole derivatives are resistant to acid/basic treatment [34,35]. PBI can be degraded under thermo-oxidative conditions but not under acid or basic hydrolysis [36,37]. In fact, PBI can be doped using basic and acidic solutions to increase electroconductivity and without observed degradation. The conditions under which PBI is stable include 0.1 M sodium hydroxide and 0.25 M hydrochloric acid [38], up to 10 M sulfuric acid and 10 M phosphoric acid for 24 h [39] and even potassium hydroxide at concentrations of 6 M [40].

One main advantage of PBI is it can also be electrospun into nanofibers, but without the need for a carrier polymer [41,42]. However, to the best of our knowledge, biocompatibility data for this material cannot be found in the literature.

The aim of this work was therefore to evaluate the biocompatibility of electrospun PBI fibers for the first time. Different doping agents were used to modify the polymer's properties, including hydrophilicity and electroconductivity. Following this, the obtained fibers were characterized. Neural stem cells were used to assess this material's biocompatibility, through proliferation and differentiation assays. The study of this material's properties aims to increase the number of available biocompatible conductive materials. Its applications are numerous, including not only the design of new electric probes for DBS but also electroconductive scaffolds for drug screening and neural tissue engineering applications.

2. MATERIALS AND METHODS

2.1. Materials

The primary antibody Anti-SOX2 was obtained from Abcam. Medical glue (silastic® medical adhesive silicone type A) was obtained from Biesterfeld Spezialchemie Iberica, SL. Ultra-low attachment 24-well plates (flat bottom) were obtained from Corning. Hydrochloric acid 37% (HCL), Isopropanol, Sulfuric acid (H_2SO_4) (10 M) and sodium chloride (NaCl) were purchased from Fisher Scientific. Celazole® S26 polybenzimidazole in *N,N*-dimethylacetamide (DMAc) solution, containing 26 wt% PBI solids and 1.5 wt% lithium chloride, was purchased from PBI Performance Products. Paraformaldehyde (PFA, 4% in phosphate buffered saline (PBS), ChemCruz) was obtained from Santa Cruz Biotechnology.

Anhydrous DMAc, β-camphorsulfonic acid (CSA), 4-(2-hydroxyethyl)-1-piperazineethanesulfonic acid (HEPES), 3-(4,5-dimethylthiazol-2-yl)-2,5-diphenyltetrazolium bromide (MTT), poly(L-ornithine hydrobromide) (MW 30,000-70,000), glucose, human recombinant insulin, 2-(4-amidinophenyl)-6-indolecarbamidine dihydrochloride (DAPI), and osmium tetroxide (4% in H2O) were purchased from Sigma. Dulbecco's phosphate buffer saline (DPBS), Dulbecco's Modified Eagle's Medium (DMEM-F12 + glutamax (1X)), N2-supplement (100X), fetal bovine serum (FBS), anti-anti mixture (penicillin 10,000 units/mL, streptomycin 10,000 μg/mL) human recombinant epidermal growth factor (EGF), human recombinant fibroblast growth factor-2 (FGF-2), B27-supplement (50X), reazurin (Alamar Blue® cell viability reagent), calcein AM, LIVE/DEAD™ Fixable Red Dead Cell Stain Kit, normal goat serum (10%), triton-x-100 (Surfact-Amps®, 10% in water), primary antibodies Anti-Tuj1 (mouse), Anti-GFAP (rat) and Anti-Nestin (mouse), secondary antibodies Alexa 488 anti-mouse, Alexa 546 anti-rat and Alexa 546 anti-rabbit, High-Capacity cDNA Reverse Transcription Kit, MicroAmp Fast Optical 96-well reaction plates and TaqMan® assays for Tuj1 (Hs00801390_s1), GFAP (Hs00909233_m1), Nestin (Hs04187831_g1), SOX2 (Hs01053049_s1) and GAPDH (Hs02786624_g1) were obtained from Thermofisher. RNA extraction kit was purchased from Zymo scientific. A frozen stock of ReN-VM cells (Millipore) was used in these studies.

2.2. PBI solution preparation and film casting

PBI S26 solution was diluted to 13% with DMAc and left overnight under mechanical stirring to obtain a homogeneous solution. This solution was then casted on to a glass petri dish and left in a vacuum oven for 4 h at 120 °C to effectively remove the solvent. Finally, the films were cooled overnight under atmospheric conditions before further processing.

2.3. Sample doping

PBI was doped by immersing the samples in aqueous solutions of sulfuric acid (5 M), camphorsulfonic acid (1 M) or HEPES (1.5 M) for 24 hours. PBI soaked in a 0.41M sodium chloride aqueous solution (0.41 M) was used as the control. Finally, the samples were washed three times with distilled water and dried overnight before further processing.

2.4. Film characterization

2.4.1. Electroconductivity—Four 50 nm thick gold stripes were deposited using a thermal evaporation system (Edwards Coating System E 306A) to improve the electrical contact between doped PBI film samples and the measurement equipment. The electroconductivity of three different films was measured by the four-point probe method, using a current source (Keithley DC power source) and a multimeter (Agilent 34401A Multimeter). Finally, the thickness of the films was measured using a Dektak 3.21 Profilometer.

2.4.2. Contact angle—Contact angle assessments were performed by a Kruss DSA25B goniometer, using the sessile drop technique and distilled water as solvent. The spreading of the water droplet on different PBI film surfaces was assessed by measuring the contact angle

of the droplet with the surface (n = 3). Drop Shape Analysis 4 Software was used to take measurements every 5 s during 2 min.

2.5. Electrospinning

A 10 mL Luer lock syringe containing the 13% PBI solution was connected by a PTFE tubing to a 21G needle. The electrospinning process was performed under the following conditions: 30 kV DC voltage, 0.5 mL h^{-1} flow rate, 16 cm from the tip of the needle to the static aluminium collector, temperature of 21°C and relative humidity of 50-55%. Samples were then left overnight to dry in atmospheric conditions and then doped as described in Section 2.3. before further processing.

2.6. Scanning Electron Microscopy (SEM)

The morphology of the electrospun fiber mats was evaluated using SEM (Carl Zeiss Supra 55 FESEM) at 1 kV, after coating with a thin layer of platinum. The average diameter of the electrospun fiber samples was determined from SEM pictures of 100 individual fibers (25,000X, 20 fibers per each of 5 images) using NIH ImageJ software (National Institute of Health, MD, USA).

2.7. Attenuated Total Reflectance–Fourier Transform Infra-Red Spectroscopy (ATR-FTIR)

ATR-FTIR spectra with 4 cm-1 resolution were obtained using Perkin Elmer Spectrum One FT-IR Spectrophotometer at room temperature. Transmittance was recorded from 650 to 4000 cm-1 wavenumbers with an accumulation of 32 scans.

2.8. Thermogravimetric Analysis (TGA)

Thermal decomposition of the fiber mats was studied under a nitrogen/oxygen atmosphere (80:20) using a computer-controlled TA instrument TGA (TGA Q5, New Castle, DE, USA) under a nitrogen/oxygen atmosphere (80:20). Samples placed in alumina crucible were heated up to 150 °C for drying (10 min) at a heating rate of 20 °C min-1 and cooled back to room temperature. The dry samples were then subjected to thermal decomposition starting from 25 °C to 1000 °C at a heating rate of 1.5 °C min^{-1}. For TGA, Profiles of mass loss as a function of temperature were obtained and evaluated using TA Universal Analysis 2000 software (Version 4.5A, TA Instruments). The onset temperature of degradation and corresponding mass losses were calculated for each sample using first and second derivatives.

2.9. ISO 10993 Cytotoxicity assays

Cytotoxicity tests were performed for electrospun PBI fibers (not doped) following the recommendations of ISO 10993-5 and 10993-12 guidelines. Briefly, mouse fibroblast cell line L-929 were cultured in Dulbecco's modified eagle's medium (DMEM + 10% FBS + 1% Anti-Anti) at 37 °C and 5% CO_2 until confluence before passage to 24-well plates at 150.000 cells cm^{-2} (direct contact) or 80.000 cells cm^{-2} (indirect contact). PBI fibers and latex (positive control) were sterilized with UV before further processing or incubated in Dulbecco's modified eagle's medium for 24 hours (6 cm^2 mL^{-1}) for lixiviate extraction (indirect contact). For direct contact, PBI fibers and latex were then placed on top of cell's

monolayer for 24 hours before image analysis on an optical microscope (Leica microsystems CMS GmbH). For indirect contact L-929 cells were incubated with lixiviates for 24 hours and cell viability was quantified using MTT assay. Briefly, after PBS washing cells were incubated with MTT solution (1 mg mL^{-1}) and left incubating for 2 hours at 37 °C. The resulting formazan salt was then dissolved using 0.1 M HCl in isopropanol and absorbance was quantified at 570 nm. Cell viability was calculated using the negative control as the reference.

2.10. ReN-VM cell culture conditions

ReN-VM cells were used as a cell model of NSC. They were grown on poly-ornithine (20 μg mL^{-1}) and laminin (10 μg mL^{-1}) coated plates in supplemented N2 medium at 37 °C and 5% CO_2 as recommended[2]. N2 medium is composed of DMEM/F12 with N2 supplement (1:100) additional glucose (1.6 g mL^{-1}), insulin (20 μg mL^{-1}) and pen-strep (1:100). N2 medium was then supplemented with EGF (20 ng mL^{-1}), FGF-2 (20 ng mL^{-1}) and B27 (20 μL mL^{-1}).

2.11. ReN-VM cell proliferation and differentiation assays and kinetic data calculation

First the electrospun fiber mats, fixed to glass coverslips with medical glue, were UV sterilized for 1.5 h per scaffold side and treated with 1% anti-anti solution in PBS for 3 h. They were then coated with poly-ornithine and laminin before seeding with ReN-VM cells (P10) at 20,000 cells cm^{-2}. Medium was added 1 h after seeding (37 °C and 5% CO_2) to promote initial cell attachment. The medium was exchanged on day 1, and every two days thereafter for 10 days duration until the end of the proliferation assay. Cellular metabolic activity was assessed using Alamar Blue® at days 3, 5, 7 and 10 for the proliferation assay. Equivalent cell number was determined using a calibration curve. Growth rate and doubling time were calculated by equations 1 and 2, respectively, assuming (after data examination) exponential phase from day 3 to day 10.

$$Growth\ rate = \frac{[\ln(cells\ day10) - \ln(cells\ day3)]}{7days} \quad \text{eq. 1}$$

$$Doubling\ time = \frac{\ln 2}{Growth\ Rate} \quad \text{eq. 2}$$

2.12. LIVE/DEAD staining and SEM imaging

At the end of the proliferation assay, cells were washed once with DPBS and then incubated with a staining solution composed of Calcein (4 μM), Fixable Red Dead Cell Stain Kit (1 μL mL^{-1}) and glucose (0.056 M) in DPBS, for 20 min at 37 °C. Cells were then washed, kept in DPBS supplemented with glucose (0.056 M) and imaged using a confocal microscope (Zeiss LSM 510META Spectral Confocal). After being fixed with paraformaldehyde (PFA) 4%, cells were treated with 1% osmium tetroxide for 30 min in a qualified fume-hood, dried using a critical point dryer (Supercritical automegasamdri 915B, purge at 3), coated with platinum and imaged using SEM (Carl Zeiss Supra 55 FESEM).

2.13. ReN-VM cell differentiation assay

Cells (56,000 cells cm^{-2}) were left to grow in the same conditions as the proliferation assay before switching N2 media for N2B27 media, inducing spontaneous differentiation of ReN-VM cells. N2B27 medium is composed of a 1:1 mixture of N2 medium (no growth factors added) and B27 medium. The B27 medium is composed of Neurobasal medium, B27 supplement (2:100), Glutamax (1:100) and pen-strep (1:200). Media was exchanged every two days until the end of the assay. Cellular metabolic activity was assessed using Alamar Blue® on days 1, 2, 4 and 8 to evaluate the number of cells present on the fibers.

2.14. Immunochemistry

After the differentiation assay, cells samples from days 4 (end of proliferation) and 8 (end of differentiation) were fixed in PFA 4% for 10 min. They were then washed with DPBS twice and permeabilized with blocking solution (goat serum 10% and Triton-x-100 0.2% in DPBS) for 15 min at RT. After another washing with DPBS, cells were incubated with Anti-Tuj1 (1:400), Anti-GFAP (1:250), Anti-Nestin (1:250) and Anti-SOX2 (1:100) diluted in staining solution (goat serum 5% and Triton-x-100 0.1% in DPBS) overnight at 4 °C. This was followed by incubation of the secondary antibodies Alexa 488 anti-mouse (1:250), Alexa 546 anti-rat (1:250) and Alexa 546 anti-rabbit (1:250) diluted in staining solution for 1 hour at RT. Finally, DAPI (1 mg mL^{-1}) diluted in staining solution was added for 5 min at 37 °C. Cells were then washed, kept in DPBS and imaged using a confocal microscope (Zeiss LSM 510META Spectral Confocal). The obtained image stacks were then merged using ImageJ.

2.15. qPCR

Quantitative real-time polymerase chain reaction (qPCR) was performed using TaqMan® gene expression assays. Tuj1 (neurons), GFAP (astrocytes), Nestin (NSCs) and SOX2 (stem cells) were chosen as the main interest targets. Gene expression in each group of the differentiation assay (days 4 and 8) was determined using the comparative Ct method and by normalizing the expression of each target gene to the endogenous reference transcript GAPDH.

2.16. Statistical analysis

All data are presented as mean values ± standard deviations (sd). Statistical analysis was performed using Microsoft Excel. Significant differences between groups were measured using ANOVA test, followed by post-hoc analysis and Bonferroni correction. $p < 0.05$ was considered statistically significant.

3. RESULTS AND DISCUSSION

3.1. Film contact angle and electroconductivity

PBI films were used to assess the effects of doping treatments on their electroconducting and surface properties. In this work, after an initial screening, 3 different acids with different pKas were chosen to test the modification of the polymer's electroconductivity: H_2SO_4, CSA and HEPES. Doping PBI with strong acids enables the modification of the polymer's

properties, while the use of a NaCl solution is expected not to. Considering tissue engineering applications, contact angle is essential to evaluate surface wettability [43]. Electroconductivity changes, important for neural cell therapy applications, were also investigated.

Changed in PBI's contact angle were observed (Table 1 and Figure S1). Treatment with sulfuric acid increased PBI's hydrophilicity, as a reduction in the contact angle from 45° to 39° was observed. The opposite was observed when PBI was treated with the organic acids CSA and HEPES, leading to an increase in contact angle to 51° and 71°, respectively. Treatment of the films with NaCl (saline control) led to an increase in the contact angle (from 45° to 60°). Apart from HEPES treated samples, the variations observed versus untreated PBI films were not statistically significant.

Changes in electroconductivity were also observed. PBI films' electroconductivity averaged 9.0×10^{-8} S cm^{-1}. When treated with H_2SO_4, electroconductivity increased to 2.4×10^{-4} S cm^{-1}, almost 10,000 times more than pristine PBI. Similar changes were reported in the literature[39,44]. When treated with other weaker acids (CSA and HEPES) and NaCl, we were not able to determine the films electroconductivity. These samples are less conductive than pristine PBI, and were labeled as "Low". We believe the bulk size of the doping agents used does not favor charge transport across PBI's chains and hence compromises the materials electroconductivity. However, the immobilization of small organic molecules as doping agents in PBI opens the possibility of immobilizing other biopolymers and bioactive within PBI. Examples of this include hyaluronic acid, dextran sulfate and deoxyribonucleic acid (DNA) and are useful for tissue engineering applications [45-47] .

3.2. Average fiber diameters

We successfully prepared nanofibers from a PBI 13% DMAc solution by electrospinning, with fibermats showing some beads. Previous reports in the literature refer bead formation, which was even regarded as a hallmark in PBI nanofiber formation[41]. Environmental conditions also played a major role in fiber formation. High relative humidity values (above 50%) were necessary for fiber formation. Humidity can therefore stabilize PBI fibers formation, and this observation is consistent with results obtained by other groups [41,48,49]. However, no explanation has yet been proposed for this phenomenon. DMAc, the solvent used to solubilize PBI, has a boiling point of 165 °C and is miscible with water. Most likely, removal of DMAc from the on-producing fibers might have been accelerated by the high humidity, in a phenomenon that might resemble the phase-inversion method used for PBI membrane [50,51]. This eased the fiber formation process and explains why no fibers were obtained when humidity was lower than 50%.

Fibers obtained upon PBI solution electrospinning have diameters within the nano-scale range (Table 1 and Figure 1). After their production, fibers were doped in the same way as the films: the obtained fibers were immersed in a concentrated acidic solution for 24 h, following Glipa X. *et al.* protocol [39]. Both high concentration and long exposure time promote extensive doping of the polymer chain, enabling efficient physical properties change such as the electroconductivity and contact angle [39,52].

Average diameter for untreated PBI fibers was 131 ± 37 nm and for NaCl treated was 139 ± 39 nm, which were not statistically different from each other. The increase in fiber average diameter was significant in the fibers treated with H_2SO_4 (204 ± 65 nm), CSA (203 ± 67 nm) and HEPES (183 ± 44 nm). The statistically significant changes observed in the fibers' diameters can have various possible explanations, including the direct incorporation of the bulky doping agents inside the fibers and between PBI chains, the electrostatic repulsion between charged amine groups and direct water retention. In fact, PBI is a hygroscopic material, and the change in the molecule's charge due to doping is also predicted to enable the samples' ability to retain more water, contributing to their diameter increase (swelling effect) [44]. Interestingly, only treatment of the fibers with acidic solutions lead to increase on PBI fibers' diameter, whereas NaCl treatment did not produce any statistically significant differences. This means that the presence of the doping agent inside PBI and changes in charge are the most plausible explanation for these changes. Finally, considering their small average diameter (inferior to 283 nm) is expected, according to literature, that the use of these fibers will enhance the proliferative potential of the cells [53].

3.3. Fiber's physical properties: ATR-FTIR and TGA

Successful doping of the PBI fibers was also confirmed by FTIR and TGA. FTIR spectra of PBI electrospun fibers, with and without doping, are depicted in Figure 2. Spectra for pristine PBI and PBI treated with NaCl are very similar, confirming that doping is not possible with saline solutions. PBI spectra have intense aromatic peaks at 693 cm^{-1}, 799 cm^{-1} and 1000 cm^{-1} corresponding to a substituted benzene ring, whereas PBI-NaCl only lacks the peak at 1000 cm^{-1}. Peaks at 1442 cm^{-1} and 1657 cm^{-1} are also visible in PBI and PBI - NaCl spectra and correspond to in plane deformation of PBI ring and of the benzimidazole ring respectively. Finally, a small peak at 2933 cm^{-1}, which is attributed to a secondary amine salt group, and a wide region between 3000 cm^{-1} and 3650 cm^{-1} associated with amine groups widely distributed through the polymer's structure are visible in the spectra. Neither PBI or PBI-NaCl show ammonium ion and amine salt peaks at 1397 cm^{-1} and 2800/2918 cm^{-1} respectively. We correlate this to the absence of effective doping of the samples.

Sulfuric acid has a pKa of −3.9 and was previously described as a good doping agent for PBI[39]. Amine groups of PBI are protonated, forming ammonium groups that change the resonance structure of the polymer[39]. In this work we hypothesize that other organic acids such as CSA (pKa = 1.2) and HEPES (pKa = 3.0), which are stronger acids than PBI (pKa = 5.23) could also serve as dopants [54].

For the samples treated with H_2SO_4 and CSA, aromatic peaks appeared at lower wavenumbers, namely at 878 cm^{-1}, and in the wide area between 910 cm^{-1} and 1210 cm^{-1}. The peak at 1442 cm^{-1} for PBI's ring deformation and the one at 1657 cm^{-1} for the benzimidazole ring are still visible. Right next to them new peaks can be identified at 1397 cm^{-1} and 1539 cm^{-1} corresponding to ammonium and secondary anime salt groups respectively, both present in doped PBI. Finally, intense amine salt peaks at 2800 cm^{-1} and 2918 cm^{-1}, along with a narrower amine peak at 3300 cm^{-1} are visible. HEPES' spectrum mixes features of both doped and undoped PBI samples, namely 2 broad aromatic (between

910 cm^{-1} and 1210 cm^{-1}) and amine peaks (3300 cm^{-1} area). Full doping does not occur for PBI-HEPES, as indicated by the low intensity peaks for amine salt at 2800 $cm^{-}1$ and 2918 cm^{-1}, evidencing that HEPES couldn't protonate PBI and therefore couldn't stabilize its resonance structure.

TGA data (Figure 3 and Table S1) is different for fibers of pristine PBI and the doped ones. In our analysis, in order to better study PBI's degradation profile, water was previously removed from the samples through a heating cycle. Therefore, no water loss was observed on the samples as reported before in the literature[41]. When compared with neat PBI, mass loss for samples PBI-CSA and PBI-HEPES start earlier (first onset temperatures 298.6 °C and 255.9 °C, respectively). This is possibly due to an oxidative degradation of the doping agents or even to a loss of volatile components due to polycondensation reactions, and then followed by PBI's chain degradation. For PBI-H_2SO_4, mass loss coincided with PBI's (414.9 °C vs 418.4 °C). For pristine PBI, three onset temperatures (418.4 °C, 438.8 °C and 469.2 °C) were observed, whereas for the remaining samples their single onset temperature were close to 429.9 ± 17.2 °C. It is plausible then to assume that the doping agents, and/or their degradation products, are at the origin of the different with the degradation processes of the doped PBI samples.

Both FTIR and TGA results demonstrate that doping is successful for H_2SO_4 and CSA treated samples, partly complete to HEPES treated samples and not effective for NaCl treated samples. This shows that doping of PBI with acids less strong than H_2SO_4 is possible but impairs electroconductivity.

3.4. Cytotoxicity assay and Cell proliferation analysis

The present work aimed at assessing PBI as a new support material for neural stem cell growth and differentiation, which can then be used in DBS probe design. To the best of our knowledge PBI's biocompatibility assessment, especially for neural tissue applications, hasn't been reported yet. Due to its chemical stability, non-degradability and ability to modify its electroconductive properties by doping, this material can also potentially be used in diverse biomedical applications, including the development of platforms for drug testing and biocompatible electronic implantable devices. It was therefore of paramount importance to assess this materials biocompatibility profile. Initially, standard ISO 10993 guidelines were followed to assess the materials biocompatibility using the murine fibroblast L-929 cell line, and the results are summarized in Figure S2. The direct contact test did not reveal major morphological changes on the cells after contact with PBI electrospun fibers. The cell viability value obtained in the indirect contact (93.4 ± 4.7%) test showed PBI electrospun fibers to have passed the biocompatibility test (cut-off 70%).

A proliferation assay with human-derived ReN-VM cells was the first approach used to assess PBI samples' biocompatibility. Figure 4 displays the average equivalent number of cells calculated from fluorescence values obtained from Alamar Blue® at different timepoints of the proliferation assay. Overall, the obtained data shows a constant increase in the number of cells for all the samples, including for the control glass coverslip samples. Proliferation data showed that ReN-VM cells were able to grow on all the samples throughout the timepoints tested. Cell numbers at day 10 show that PBI-CSA afforded a

significantly higher number of cells at day 10. Taken this data into account, we calculated the respective kinetic data between days 3 to 10 for better comparison of the samples.The kinetic data is summarized in Table 2.

The kinetic values obtained were used to better compare the different samples at the end of the experiment. Despite of the difference observed in cell numbers for Glass and all PBI samples overall growth rate values were higher on PBI fiber samples (undoped and doped), which led to shorter doubling times. We hypothesize that due to its 3D-structure and porous nature, PBI fibers can be remodeled by NSCs. This phenomenon, which appears to be independent of the doping agent used, might facilitate cell-cell contact and promote cell proliferation [55-57]. LIVE/DEAD images (Figure 5(A)) of cells at day 10 show high viability of the cells by the end of the experiment. SEM images (Figure 5(B)) show ReN-VM cells with their normal spindle/stellar shape adhered to the fiber mat, confirming that these cells were viable at the time they were fixed.

Previous research from Alba *et al.* shows that cell interaction with PEDOT-coated DBS probes is important for tissue integration and better signal recording. Our material shows promising applications as a material for DBS or neural tissue engineering for the same reasons [12]. Overall, the previous data evidences that PBI is biocompatible towards ReN-VM cell expansion. Considering the favorable kinetic profile and the viability of the cultured cells, PBI-CSA samples was chosen for further studies.

3.5. Cell differentiation

In order to explore further PBI's biomedical applications, ReN-VM cells were differentiated on PBI-CSA fibers. PBI-CSA was chosen for these studies due to the higher growth rate value obtained. This allowed to evaluate the potential use of doped PBI in cell culture, which can be reproduced with other doping agents such as sulfuric acid and phosphoric acid depending on the envisaged application. The protocol included a 4-days proliferation period, followed by another 4-days period of differentiation. During this time, change from the supplemented N2 media used for proliferation to N2B27 media, not supplemented, allowed the spontaneous differentiation of ReN-VM cells. The equivalent number of cells was also assessed throughout the process (Figure S3).

Immunochemistry was used to evaluate neural gene expression (Figure 6). At day 4, for both samples, no signal was detected for Tuj1, and for GFAP had a low signal intensity. High intensity signals for both SOX2 and Nestin were also identified at day 4. There were visible changes at day 8, 4 days after differentiation was induced, namely in cell morphology and marker expression. As for cell's morphology, differentiated ReN-VM cells were able to spread through both substrates, without any specific orientation, were more elongated and established a mesh of prolongments between neighbor cells. While the cells were still expressing Nestin and SOX2 at similar or lower intensities, both GFAP and Tuj1's signals substantially increased. Both GFAP and Tuj1 are commonly associated with astrocytes and neural cells but are interchangeably expressed in both cells at the immature stage[58-60]. However, differences in staining fluorescence intensity were evident for Tuj1 and GFAP and allowed to identify cells with these markers for differentiation towards neurons and astrocytes. SOX2 and Nestin are still present in the cells at day 8. Because these markers are

specific for neural stem cells, their presence might be associated with an immature profile of the cells and/or cell undifferentiated cell populations. These observations indicate that ReN-VM cells were differentiating into neuronal cells.

Samples from days 4 and 8 were also compared towards their gene transcription activity by qPCR (Figure 7). The genes analyzed were *Sex determining region Y-box 2* (SOX2) (Ectoderm-derived stem cells), *Nestin* (NES) (Neural stem cells), *Glial fibrillary acidic protein* (GFAP) (Astrocytes) and *β-Tubulin III* (Tuj1) (Neurons). The results indicate that both cell groups growing on glass coverslips and PBI-CSA samples were able to differentiate towards neural cells. Gene transcription of SOX2, Nestin, GFAP and Tuj1 increased for all the samples from day 4 to day 8. For SOX2, statistical differences were significant between days 4 and 8 for samples PBI-CSA and glass coverslip. Concerning Nestin, again differences were observed both for samples on PBI-CSA and glass coverslips between days 4 and 8, but those were only statistically significant for the later. Concerning GFAP, increased expression in both PBI-CSA and glass coverslip samples from day 4 to 8 were both statistically significant. Finally, for Tuj1 no statistically significant differences were observed between the samples, despite the visible increase in gene expression for both samples between the two time points.

The results obtained from the qPCR experiments are in line with the immunostaining observation. Overall, gene expression of all the genes tested increased from day 4 to day 8, even SOX2 and Nestin. This is correlated to an immature profile of the cells, an increase in these genes' expression is expected because of the short differentiation time. However, since GFAP and Tuj1 RNA levels increase during the same timeframe, indicating early neural commitment, we could confirm that the differentiation process was taking place.

3.6. Final considerations

When considering biocompatibility alone, PBI fibers (with or without doping) performed better than glass coverslips regarding cell proliferation and differentiation. However, from an application point of view, differences between the two must be considered. PBI is a thermal and chemical-resistant polymer that can be easily processed into various flexible structures (fibers and films) and its physico-chemical properties, such as contact angle and electroconductivity, can be fine-tuned by chemical doping. Although in this work we restricted the study only to three doping agents, other effective agents such as phosphoric acid should also be used.

The most abundant type of enzymes, present in the human extracellular environment, catalyzes the cleavage of esters (e.g., lipases), glycosidic (e.g., lysozyme) and peptidic bonds (e.g., metalloproteases) and these are responsible for the extracellular matrix homeostasis [66-68]. Because this polymer's structure does not resemble any major biological molecules nor does it have any ester bonds in its structure, we do not expect PBI to biodegrade easily. Nevertheless, future studies should include a biodegradation profile assessment to determine this materials' full potential in the field of biomedicine.

PBI shows promise in future biomedical applications based all their studied features. Examples include the construction of electroconductive platforms for cultured cell

stimulation suitable for cell expansion and the creation of in vitro models suitable for disease progression studies and drug screening. Due to the biocompatibility profile of PBI and its ability to interact with living cells, its use in DBS probes also presents another promising application. With regard to tissue engineering applications, PBI can also be viewed as a suitable candidate for the construction of electroconductive scaffolds/platforms for replacing electrically active organs (e.g. brain, heart) or even controlled drug delivery.

4. CONCLUSIONS

In summary, PBI fibers were successfully electrospun, doped with different acids and characterized by FTIR and TGA. Doping PBI with strong acids increased the fibers' diameter, and its effects on electroconductivity and contact angle depended on the acid used. Both pristine and doped PBI fibers were able to support ReN-VM proliferation and the cells managed to keep their normal spindle/stellar morphology. When induced, ReN-VM cells were also able to differente in neural cells on PBI-CSA fibers, showing a neuronal-like morphology and expressing neural cell markets. This work demonstrates that PBI is a biocompatible electroconductive polymer. These results open the way for the application of PBI in the design of neural cell friendly platforms. These include not only DBS electrodes and other devices for man-machine interface, but also electroconductive scaffolds for tissue engineering applications and drug screening platforms.

Supplementary Material

Refer to Web version on PubMed Central for supplementary material.

ACKNOWLEDGEMENTS

The authors express gratitude to the Center for Biotechnology & Interdisciplinary Studies (CBIS), as well as the following CBIS core directors and the staff for their assistance in handling characterization instruments ad data analysis: Analytical core facility (Joel Morgan, PhD), Microscopy Research (Sergey Pryshchep, PhD) and Nanoscale characterization (Deniz Rende, PhD). The authors also thank the assistance from all the personnel from MNCR-cMDIS-RPI cleanroom facility for SEM (Mr. David Frey, BSc) and 4-proble analysis (Bryant Colwill, BSc; Sarah An, PhD; John Barthel, BSc).

F.F.F. Garrudo and J.C. Silva gratefully acknowledge the financial support from FCT (Fundação para a Ciência e Tecnologia) through the scholarships PD/BD/114045/2015 and SFRH/BD/105771/2014 respectively. F. A. Ferreira acknowledges the financial support from CNPq-Brasil through the scholarship 205201/2014-8.

The authors acknowledge the funding received by iBB - Institute for Bioengineering and Biosciences from FCT (UID/BIO/04565/2013) and from Programa Operacional Regional (POR) Lisboa 2020 (Project N. 007317) and by IT from FCT(UID/EEA/50008/2019). We also thank the funding received from POR Lisboa 2020 through the project PRECISE - Accelerating progress toward the new era of precision medicine (Project N. 16394) and to FCT through the project NEURON, PTDC/CTM-CTM/30237/2017. This work is also funded by the US National Institutes of Health, grant # DK111958 and New York State grant # SCRIB DOH01-PART2-2017.

REFERENCES

[1]. Pettikiriarachchi J, Parish C, Shoichet M, Forsythe J, Nisbet D, Biomaterials for Brain Tissue Engineering, Aust J Chem. 63 (2010) 1143–1154.

[2]. Pires F, Ferreira Q, Rodrigues C, Morgado J, Ferreira F, Neural stem cell differentiation by electrical stimulation using a cross-linked PEDOT substrate: Expanding the use of biocompatible conjugated conductive polymers for neural tissue engineering, Biochimica et Biophysica Acta (BBA) - General Subjects. 1850 (2015) 1158–1168. [PubMed: 25662071]

[3]. Yang K, Yu S, Lee J, Lee H-R, Chang G-E, Seo J, et al., Electroconductive nanoscale topography for enhanced neuronal differentiation and electrophysiological maturation of human neural stem cells, Nanoscale. 9 (2017) 18737–18752. [PubMed: 29168523]

[4]. Neumann W-J, Turner R, Blankertz B, Mitchell T, Kühn A, Richardson R, Toward Electrophysiology-Based Intelligent Adaptive Deep Brain Stimulation for Movement Disorders, Neurotherapeutics. 16 (2019) 105–118. [PubMed: 30607748]

[5]. Roy H, Green A, Aziz T, State of the Art: Novel Applications for Deep Brain Stimulation, Neuromodulation Technology Neural Interface. 21 (2018) 126–134.

[6]. Bittlinger M, Müller S, Opening the debate on deep brain stimulation for Alzheimer disease-a critical evaluation of rationale, shortcomings, and ethical justification, BMC Medical Ethics. 19 (2018) 1–23. [PubMed: 29304784]

[7]. Mann A, Gondard E, Tampellini D, Milsted J, Marillac D, Hamani C, et al., Chronic deep brain stimulation in an Alzheimer's disease mouse model enhances memory and reduces pathological hallmarks, Brain Stimulation. 11 (2018) 435–444. [PubMed: 29246746]

[8]. Koppes A, Seggio A, Thompson D, Neurite outgrowth is significantly increased by the simultaneous presentation of Schwann cells and moderate exogenous electric fields, J Neural Eng. 8 (2011) 046023. [PubMed: 21712572]

[9]. Zhu W, Ye T, Lee S-J, Cui H, Miao S, Zhou X, et al., Enhanced Neural Stem Cell Functions in Conductive Annealed Carbon Nanofibrous Scaffolds with Electrical Stimulation, Nanomedicine: Nanotechnology, Biology and Medicine. 14 (2017) 2485–2494.

[10]. Sensharma P, Madhumathi G, Jayant RD, Jaiswal AK, Biomaterials and cells for neural tissue engineering: Current choices, Materials Science and Engineering C. 77 (2017)1302–1315. [PubMed: 28532008]

[11]. Kim S, Lee H, Kim Y, Neural stem cell-based treatment for neurodegenerative diseases, Neuropathology. 33 (2013) 491–504. [PubMed: 23384285]

[12]. Alba N, Du Z, Catt K, Kozai T, Cui X, In Vivo Electrochemical Analysis of a PEDOT/MWCNT Neural Electrode Coating, Biosensors. 5 (2015) 618–646. [PubMed: 26473938]

[13]. Kozai TDY, Jaquins-Gerstl AS, Vazquez AL, Michael AC, Cui XT, Brain tissue responses to neural implants impact signal sensitivity and intervention strategies, ACS Chem Neurosci. 6 (2015) 48–67. [PubMed: 25546652]

[14]. Kim D-H, Wiler J, Anderson D, Kipke D, Martin D, Conducting polymers on hydrogel-coated neural electrode provide sensitive neural recordings in auditory cortex, Acta Biomaterialia. 6 (2010) 57–62. [PubMed: 19651250]

[15]. Ganji M, Kaestner E, Hermiz J, Rogers N, Tanaka A, Cleary D, et al., Development and Translation of PEDOT:PSS Microelectrodes for Intraoperative Monitoring, Advanced Functional Materials. (2017) 1700232.

[16]. Zhang K, Shi Z, Zhou J, Xing Q, Ma S, Li Q, et al., Potential application of an injectable hydrogel scaffold loaded with mesenchymal stem cells for treating traumatic brain injury, J Mater Chem B. 6 (2018) 2982–2992. [PubMed: 32254333]

[17]. Shin J, Choi E, Cho J, Cho A-N, Jin Y, Yang K, et al., Three-Dimensional Electroconductive Hyaluronic Acid Hydrogels Incorporated with Carbon Nanotubes and Polypyrrole by Catechol-Mediated Dispersion Enhance Neurogenesis of Human Neural Stem Cells, Biomacromolecules. 18 (2017) 3060–3072. [PubMed: 28876908]

[18]. Zuidema JM, Provenza C, Caliendo T, Dutz S, Gilbert R, Magnetic NGF-Releasing PLLA/Iron Oxide Nanoparticles Direct Extending Neurites and Preferentially Guide Neurites along Aligned Electrospun Microfibers, Acs Chem Neurosci. 6 (2015) 1781–1788. [PubMed: 26322376]

[19]. Garrudo FFF, Chapman CA, Hoffman PR, Udangawa RW, Silva JC, Mikael PE, et al., Polyaniline-Polycaprolactone Blended Nanofibers for Neural Cell Culture, European Polymer Journal. 117 (2019) 28–37.

[20]. Borah R, Ingavle G, Sandeman S, Kumar A, Mikhalovsky S, Electrically conductive MEH-PPV:PCL electrospun nanofibres for electrical stimulation of rat PC12 pheochromocytoma cells, Biomater Sci-Uk. 6 (2018) 2342–2359.

[21]. Akhavan O, Graphene scaffolds in progressive nanotechnology/stem cell-based tissue engineering of the nervous system, Artificial Organs. 4 (2016) 3169–3190.

[22]. Grill WM, Norman SE, Bellamkonda RV, Implanted neural interfaces: biochallenges and engineered solutions, Annu Rev Biomed Eng. 11 (2009) 1–24. [PubMed: 19400710]

[23]. Chang K-A, Kim J, Kim JA, Lee S, Lee S, Kim S, et al., Biphasic Electrical Currents Stimulation Promotes both Proliferation and Differentiation of Fetal Neural Stem Cells, PLoS ONE. 6 (2011) e18738. [PubMed: 21533199]

[24]. Balint R, Cassidy N, Cartmell S, Conductive polymers: towards a smart biomaterial for tissue engineering, Acta Biomaterialia. 10 (2014) 2341–2353. [PubMed: 24556448]

[25]. Thompson B, Richardson R, Moulton S, Evans A, O'Leary S, Clark G, et al., Conducting polymers, dual neurotrophins and pulsed electrical stimulation — Dramatic effects on neurite outgrowth, J Control Release. 141 (2010) 161–167. [PubMed: 19788902]

[26]. Xu B, Bai T, Sinclair A, Wang W, Wu Q, Gao F, et al., Directed neural stem cell differentiation on polyaniline-coated high strength hydrogels, Materials Today Chemistry. 1 (2016) 15–22.

[27]. Baji A, Mai Y-W, Wong S-C, Abtahi M, Chen P, Electrospinning of polymer nanofibers: Effects on oriented morphology, structures and tensile properties, Compos Sci Technol. 70 (2010) 703–718.

[28]. Lu W, Sun J, Jiang X, Recent advances in electrospinning technology and biomedical applications of electrospun fibers, J Mater Chem B. 2 (2014) 2369–2380. [PubMed: 32261409]

[29]. Wang J, Tian L, Chen N, Ramakrishna S, Mo X, The cellular response of nerve cells on poly-l-lysine coated PLGA-MWCNTs aligned nanofibers under electrical stimulation, Materials Science and Engineering: C. 91 (2018) 715–726. [PubMed: 30033306]

[30]. Ghasemi-Mobarakeh L, Prabhakaran MP, Morshed M, Nasr-Esfahani MH, Ramakrishna S, Electrical stimulation of nerve cells using conductive nanofibrous scaffolds for nerve tissue engineering, Tissue Engineering Part A. 15 (2009) 3605–3619. [PubMed: 19496678]

[31]. Li Y, Li X, Zhao R, Wang C, Qiu F, Sun B, et al., Enhanced adhesion and proliferation of human umbilical vein endothelial cells on conductive PANI-PCL fiber scaffold by electrical stimulation, Mater Sci Eng C. 72 (2017) 106–112.

[32]. Razak SIA, Wahab IF, Fadil F, Dahli FN, Khudzari AZM, Adeli H, A review of electrospun conductive polyaniline based nanofiber composites and blends: processing features, applications, and future directions, Adv Mater Sci Eng. (2015) 1–19.

[33]. Holland ER, Pomfret SJ, Adams PN, Monkman AP, Conductivity studies of polyaniline doped with CSA, Journal of Physics: Condensed Matter. 8 (1996) 2991–3002.

[34]. Vogel H, Marvel C, Polybenzimidazoles, new thermally stable polymers, J Polym Sci. 50 (1961) 511–539.

[35]. Sandor RB, PBI (Polybenzimidazole): Synthesis, properties and applications, High Perform Polym. 2 (1990) 25–37.

[36]. Musto FE Karasz WJ MacKnight, Fourier transform infra-red spectroscopy on the thermo-oxidative degradation of polybenzimidazole and of a polybenzimidazole/polyetherimide blend, Polymer. 34 (1993) 2934–2945.

[37]. Li H-Y, Liu Y-L, Polyelectrolyte composite membranes of polybenzimidazole and crosslinked polybenzimidazole-polybenzoxazine electrospun nanofibers for proton exchange membrane fuel cells, J Mater Chem A. 1 (2012) 1171–1178.

[38]. Ferreira F, Esteves T, Carrasco M, Bandarra J, Afonso C, Ferreira F, Polybenzimidazole for active pharmaceutical ingredient purification: The Mometasone furoate case study., Ind Eng Chem Res. (2019).

[39]. Glipa X, Bonnet B, Mula B, Deborah J, Rozière J, Investigation of the conduction properties of phosphoric and sulfuric acid doped polybenzimidazole, J Mater Chem. 9 (1999) 3045–3049.

[40]. Hou H, Sun G, He R, Wu Z, Sun B, Alkali doped polybenzimidazole membrane for high performance alkaline direct ethanol fuel cell, J Power Sources. 182 (2008) 95–99.

[41]. Anandhan, Ponprapakaran, Senthil, George G, Parametric study of manufacturing ultrafine polybenzimidazole fibers by electrospinning, International Journal of Plastics Technology. 16 (2012) 101–116.

[42]. Kim C, Kim Y-J, Kim Y-A, Fabrication and structural characterization of electro-spun polybenzimidazol-derived carbon nanofiber by graphitization, Solid State Communications. 132 (2004) 567–571.

[43]. Arima Y, Iwata H, Effect of wettability and surface functional groups on protein adsorption and cell adhesion using well-defined mixed self-assembled monolayers, Biomaterials. 28 (2007) 3074–3082. [PubMed: 17428532]

[44]. Li Q, He R, Berg R, Hjuler H, Bjerrum N, Water uptake and acid doping of polybenzimidazoles as electrolyte membranes for fuel cells, Solid State Ionics. 168 (2004) 177–185.

[45]. Wang S, Guan S, Wang J, Liu H, Liu T, Ma X, et al., Fabrication and characterization of conductive poly (3,4-ethylenedioxythiophene) doped with hyaluronic acid/poly (l-lactic acid) composite film for biomedical application, J Biosci Bioeng. 123 (2017)116–125. [PubMed: 27498308]

[46]. Harman D, Gorkin R, Stevens L, Thompson B, Wagner K, Weng B, et al., Poly(3,4-ethylenedioxythiophene):dextran sulfate (PEDOT:DS) – A highly processable conductive organic biopolymer, Acta Biomater. 14 (2015) 33–42. [PubMed: 25484333]

[47]. Dawn A, Nandi A, Biomolecular Hybrid of a Conducting Polymer with DNA: Morphology, Structure, and Doping Behavior, Macromolecular Bioscience. 5 (2005) 441–450. [PubMed: 15889390]

[48]. Walmsley R, Hlangothi P, Litwinski C, Nyokong T, Torto N, Tshentu Z, Catalytic oxidation of thioanisole using oxovanadium(IV)-functionalized electrospun polybenzimidazole nanofibers, J Appl Polym Sci. 127 (2013) 4719–4725.

[49]. Graberg T, Thomas A, Greiner A, Antonietti M, Weber J, Electrospun Silica—Polybenzimidazole Nanocomposite Fibers, Macromol Mater Eng. 293 (2008) 815–819.

[50]. Wainright JS, Wang J-T, Weng D, Savinell RF, Litt M, Acid-Doped Polybenzimidazoles: A New Polymer Electrolyte, J Electrochem Soc. 142 (1995).

[51]. Kurdakova V, Quartarone E, Mustarelli P, Magistris A, Caponetti E, Saladino ML, PBI-based composite membranes for polymer fuel cells, J Power Sources. 195 (2010) 7765–7769.

[52]. Valtcheva IB, Kumbharkar SC, Kim JF, Bhole Y, Livingston AG, Beyond polyimide: Crosslinked polybenzimidazole membranes for organic solvent nanofiltration (OSN) in harsh environments, Journal of Membrane Science. 457 (2014) 62–72.

[53]. Christopherson G, Song H, Mao H-Q, The influence of fiber diameter of electrospun substrates on neural stem cell differentiation and proliferation, Biomaterials. 30 (2009) 556–564. [PubMed: 18977025]

[54]. Li Q, Jensen JO, Savinell RF, Bjerrum NJ, High temperature proton exchange membranes based on polybenzimidazoles for fuel cells, Progress in Polymer Science. 34 (2009) 449–477.

[55]. Lu P, Takai K, Weaver VM, Werb Z, Extracellular matrix degradation and remodeling in development and disease, Cold Spring Harb Perspect Biol . 3 (2011).

[56]. Madl C, LeSavage B, Dinh C, Dewi R, Stowers R, Khariton M, et al., Maintenance of neural progenitor cell stemness in 3D hydrogels requires matrix remodelling, Nature Materials. 16 (2017) 1233. [PubMed: 29115291]

[57]. Madl CM, c Heilshorn S, Engineering hydrogel microenvironments to recapitulate the stem cell niche, Annu. Rev. Biomed. Eng. 20 (2018) 21–47. [PubMed: 29220201]

[58]. Dráberová E, Valle L, Gordon J, Marková V, Šmejkalová B, Bertrand L, et al., Class III β-Tubulin Is Constitutively Coexpressed With Glial Fibrillary Acidic Protein and Nestin in Midgestational Human Fetal Astrocytes: Implications for Phenotypic Identity, Journal of Neuropathology & Experimental Neurology. 67 (2008) 341–354. [PubMed: 18379434]

[59]. Casper K, McCarthy K, GFAP-positive progenitor cells produce neurons and oligodendrocytes throughout the CNS, Molecular and Cellular Neuroscience. 31 (2006) 676–684. [PubMed: 16458536]

[60]. Liu Namba, Liu Suzuki, Shioda Seki, Glial fibrillary acidic protein-expressing neural progenitors give rise to immature neurons via early intermediate progenitors expressing both glial fibrillary acidic protein and neuronal markers in the adult hippocampus, Neuroscience. 166 (2010) 241–251. [PubMed: 20026190]

[61]. PA Jones D-Y Research, Destruction of extracellular matrices containing glycoproteins, elastin, and collagen by metastatic human tumor cells, Cancer Research. (1980).

[62]. Vlodavsky I, Korner G, Ishai-Michaeli R, Bashkin P, Bar-Shavit R, Fuks Z, Extracellular matrix-resident growth factors and enzymes: possible involvement in tumor metastasis and angiogenesis, Cancer Metast Rev. 9 (1990) 203–226.

[63]. Nawaz M, Shah N, Zanetti B, Maugeri M, S.-R. Cells, Extracellular vesicles and matrix remodeling enzymes: the emerging roles in extracellular matrix remodeling, progression of diseases and tissue repair, Cells. (2018).

HIGHLIGHTS

- Polybenimidazole (PBI) was electrospun and doped with different acids
- Doping Polybenzimidazole was confirmed by FTIR, TGA and electroconductivity changes
- Neural stem cells can adhere and grow on all polybenzimidazole fibers
- Doped fibers supported neural stem cell differentiation into neurons and astrocytes

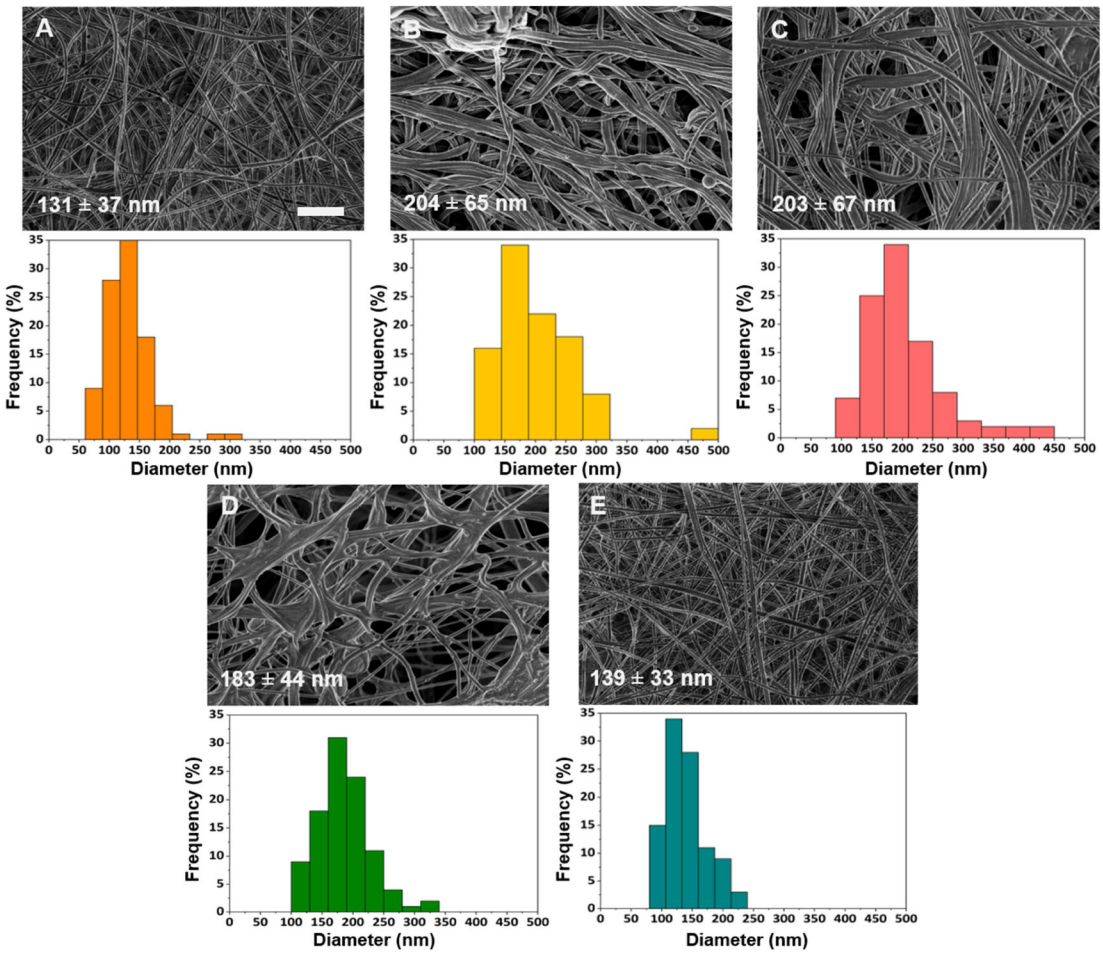

Figure 1:

SEM images and respective histograms (below) of PBI electrospun fibers. (**A**) neat PBI fibers, and fibers treated with (**B**) H_2SO_4, (**C**) CSA, (**D**) HEPES, and (**E**) NaCl (scale bar = 2 μm).

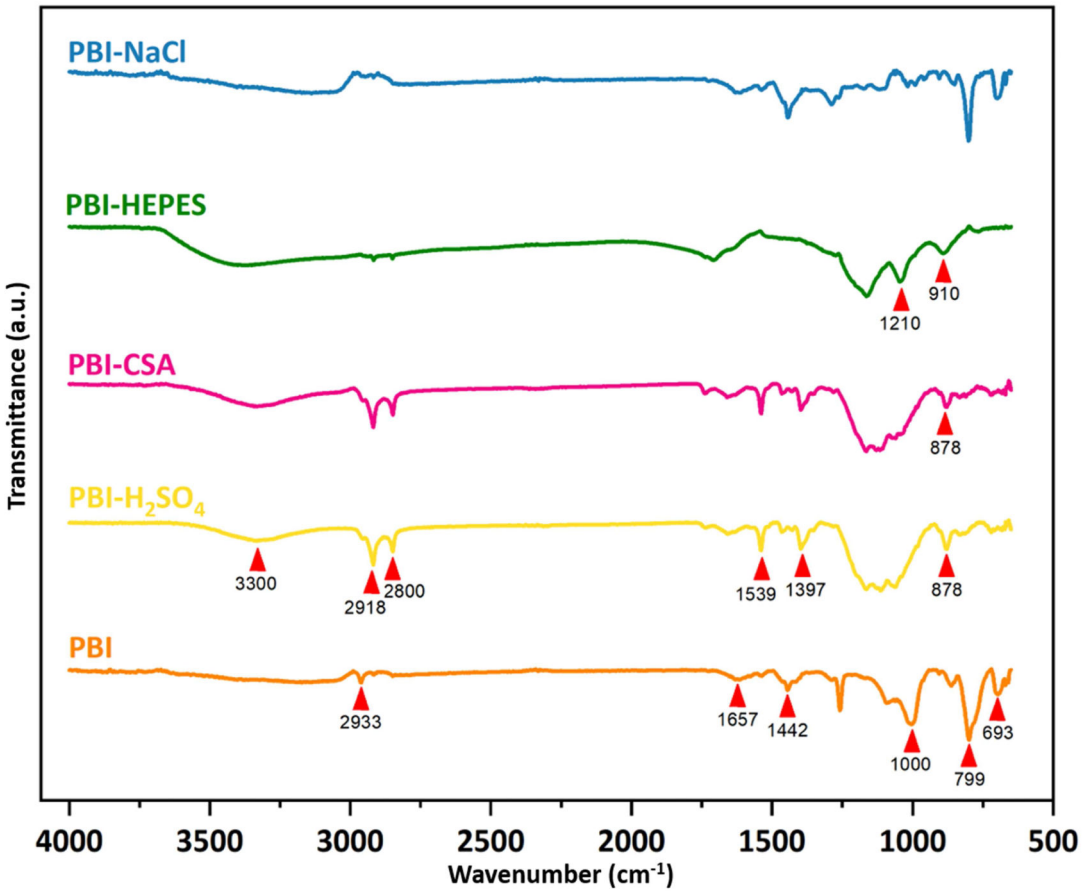

Figure 2:

ATR-FTIR profiles (Resolution 4cm-1, 32 scans) for PBI fibers with (**a**) no doping, and doped with (**b**) H_2SO_4, (**c**) CSA, (**d**) HEPES, and (**e**) NaCl.

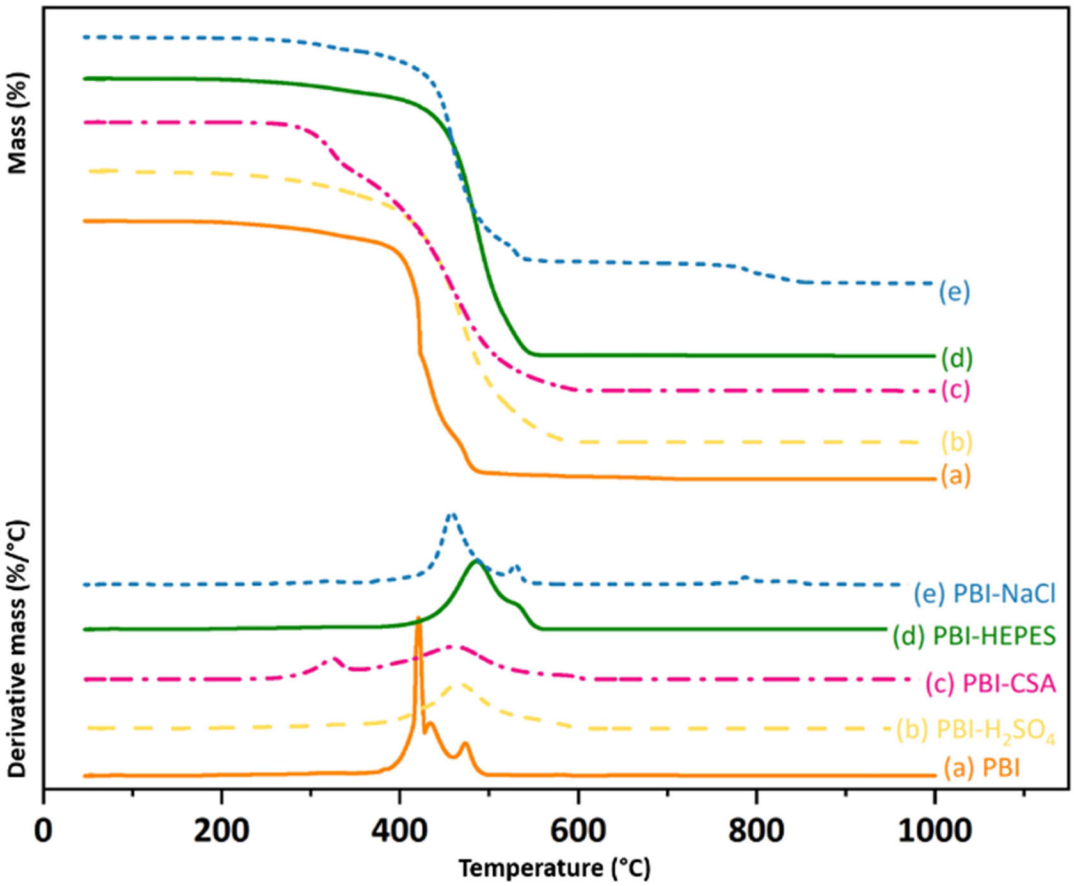

Figure 3:

(**A**) TGA profiles (1.5°C per min, 150-1000°C, with 20% oxygen) of PBI electrospun fibers, not doped or doped with H_2SO_4, CSA, HEPES and NaCl, and (**B**) respective first derivatives.

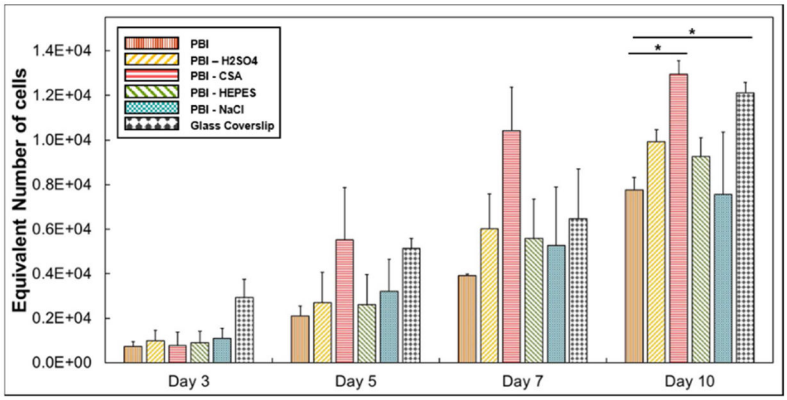

Figure 4:

Cell growth profile at days 3, 5, 7 and 10, using the equivalent number of cells (mean ± sd, n = 3) (* corresponds to $p < 0.05$). Glass coverslips used as controls.

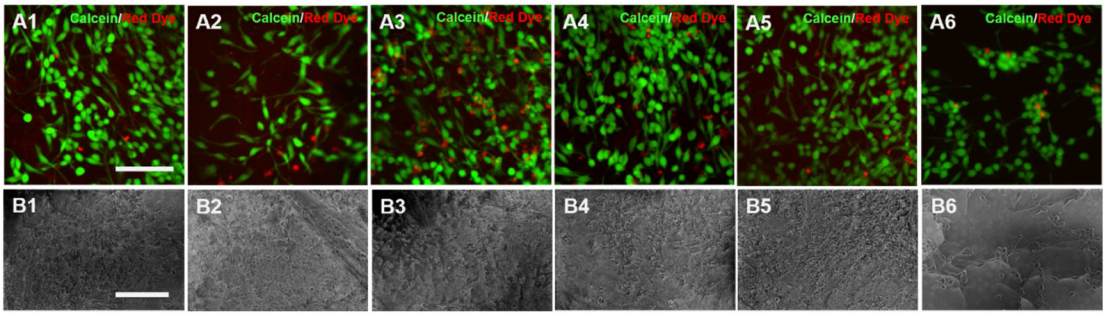

Figure 5:

LIVE/DEAD (**A**) and SEM (**B**) images of ReN-VM cells growing on PBI fibers, (**1**) with no doping, or doped with (**2**) H_2SO_4, (**3**) CSA, (**4**) HEPES, or (**5**) NaCl. Cells growing on glass coverslips (**6**) were used as controls (scale bar = 100 μm).

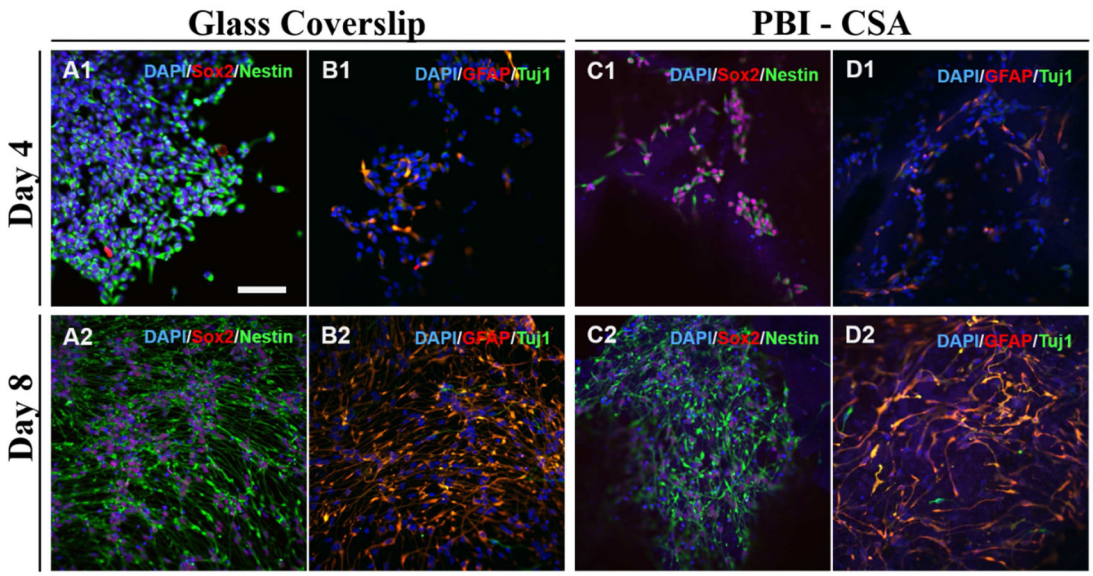

Figure 6:

Immunostaining of ReN-VM cells growing on Glass (**A, B**) and PBI-CSA samples (**C, D**) at day 4 (**1**) and 8 (**2**) (scale bar = 100 μm).

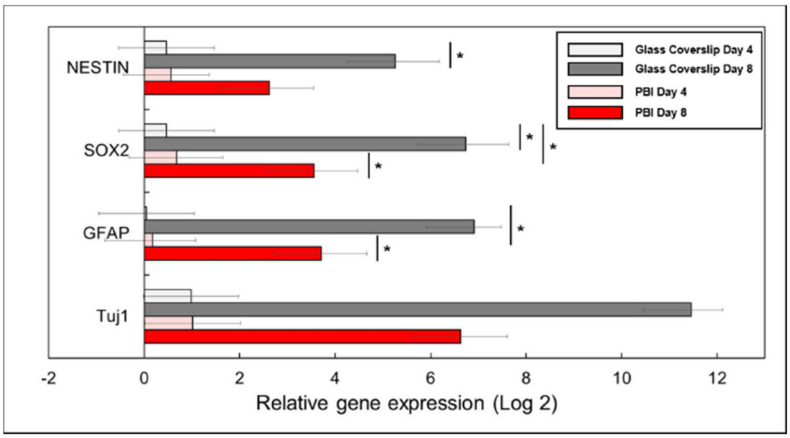

Figure 7:

qPCR analysis on gene expression of the neural genes Tuj1 and GFAP, and the neural stem cell genes NES and SOX2 (n = 2) (mean ± sd) (* = p-value < 0.05).

Table 1:

Electroconductivity and contact angle of PBI films (and diameter of the PBI electrospun fibers) (mean ± sd) (* = p-value < 0.05).

	Films		Fibers
	Contact Angle (θ)	**Electroconductivity (S cm^{-1})**	**Diameter (nm)**
PBI	44.9 ± 2.1	(9.0 ± 1.9) × 10^{-8}	131 ± 37
PBI-H_2SO_4	39.3 ± 9.7	(2.4 ± 2.2) × 10^{-4}	204 ± 65 (*)
PBI-CSA	51.3 ± 4.7	(Low)	203 ± 67 (*)
PBI-HEPES	70.6 ± 4.2 (*)	(Low)	183 ± 44 (*)
PBI-NaCl	59.9 ± 8.6	(Low)	139 ± 33

Table 2:

Cell kinetic data, including growth rate and doubling time, for ReN-VM cells growing on different PBI fibers and glass coverslips.

	Growth Rate (day^{-1})	Doubling Time (h)
PBI	0.34 ± 0.06	49.5 ± 8.0
PBI-H_2SO_4	0.33 ± 0.08	50.4 ± 13.9
PBI-CSA	0.46 ± 0.18	41.4 ± 13.6
PBI-HEPES	0.35 ± 0.08	50.0 ± 13.3
PBI-NaCl	0.28 ± 0.01	59.5 ± 2.9
Glass Coverslip	0.20 ± 0.05	83.2 ± 18.9